Journal of Power Sources 215 (2012) 170–178

Contents lists available at SciVerse ScienceDirect

Journal of Power Sources

journal homepage: www.elsevier.com/locate/jpowsour

Effect of glutaric anhydride additive on the $LiNi_{0.4}Mn_{1.6}O_4$ electrode/electrolyte interface evolution: A MAS NMR and TEM/EELS study

Zhongli Wang [a], Nicolas Dupré [a,*], Luc Lajaunie [a], Philippe Moreau [a], Jean-Frédéric Martin [b], Laura Boutafa [b], Sébastien Patoux [b], Dominique Guyomard [a]

[a] Institut des Matériaux Jean Rouxel, CNRS UMR 6502, Université de Nantes, France
[b] LITEN, CEA, Grenoble, France

HIGHLIGHTS

- Change of composition of interphase at high potential.
- Glutaric anhydride promotes the formation of fluorophosphates.
- Flurophosphates are more stable than LiF on the surface of active material.
- Additive does not prevent dissolution of Mn from the active material.

ARTICLE INFO

Article history:
Received 9 March 2012
Received in revised form
13 April 2012
Accepted 6 May 2012
Available online 18 May 2012

Keywords:
Lithium batteries
Positive electrode
Interface
NMR

ABSTRACT

Investigation of electrode/electrolyte interface of 5V spinel material $LiNi_{0.4}Mn_{1.6}O_4$ was carried out in the presence of glutaric anhydride additive, using combined magic angle spinning NMR spectroscopy and electron energy-loss spectroscopy. After exposure to $LiPF_6$ in EC/DMC liquid electrolyte, oxidation state of +III or lower has been evidenced by EELS for Mn ions, indicating that the presence of glutaric anhydride additive in the electrolyte, not only modifies the interphase, but does not prevent chemical reactions with the active material. Further investigation of the influence of the additive upon storage and cycling was performed using combined ^7Li and ^{19}F MAS NMR. The native interphase formed by simple contact of the active material with the electrolyte is partially destroyed at high potential but the new appearing interphase is overall increasing upon cycling, independently from the presence of glutaric anhydride. The use of glutaric anhydride is nevertheless beneficial as it clearly restrains the formation of lithiated interphasial species and alters the interphase composition since the formation of fluorophosphates is promoted, lowering the relative amount of resistive LiF. Although resistive LiF can be formed in significant amount, it is removed by the DMC rinsing while fluorophosphates display a stronger adherence to the active material.

1. Introduction

Lithium ion batteries are today the most promising power source of the portable electronic devices [1]. Compared with lead-acid and nickel-MH batteries, a lithium battery has higher power and energy, making it appropriate for cell phones and laptop computers. Energy, power, safety and cost are however still issues for its application in electric vehicles [2–5]. For applications requiring high energy density, high voltage spinel oxides are promising candidates. In this respect, D. Guyomard [6,7], K. Amine [8] and J.R. Dahn [9] proposed the family of $LiMn_{2-x}M_xO_4$ spinel oxides (M=Cr, Fe, Ni) operating around 5 V. Among these, intensive efforts were devoted to the development of $LiNi_{0.5}Mn_{1.5}O_4$. Very recently optimization of electrochemical performance led to the selection of the $LiNi_{0.4}Mn_{1.6}O_4$ composition for future developments. This composition shows the highest discharge capacity and a better capacity retention than $LiNi_{0.5}Mn_{1.5}O_4$ [10,11]. For high voltage spinel compounds, the main issue is the electrolyte instability at high voltage that can

* Corresponding author. Tel.: +33 (0) 2 40 37 39 33; fax: +33 (0)2 40 37 39 95.
E-mail address: nicolas.dupre@cnrs-imn.fr (N. Dupré).

0378-7753/$ – see front matter © 2012 Elsevier B.V. All rights reserved.
doi:10.1016/j.jpowsour.2012.05.027

lead to large capacity loss due to self-discharge and irreversibility [12–16]. The major challenge clearly comes from the electrolyte/electrode interface, where the highly oxidative voltage close to 5 V vs Li^+/Li at the end of charge leads to the decomposition of both inorganic salt and organic solvents and the presence of decomposition products, including LiF, fluorophosphates and organic species on the surface of the active material particles. This essential electrolyte/electrode interface has been named solid electrolyte interphase (SEI) [17] and is expected to determine the kinetics of Li ion intercalation [18–23]. Two approaches are typically envisaged to design electrolytes with improved tolerance to higher potential. Electrolytes using new solvents such as sulfones [24,25] or nitriles [26] seem promising altermnatives to carbonates in this regard. On the other hand, the trace presence (<5%) of additives diplaying redox properties tailored for 5V applications [27,28] is expected to result in their complete consumption during the interphase forming cycle, leaving no impact on the bulk properties of the electrolyte such as cost or viscosity [29]. This second approach, considered as the most economic and effective method for the tailoring of interphases has been chosen for the present work. Anhydrides, such as glutaric anhydride, are used in applications such as corrosion inhibitors and surfactants. The in-situ formation of a stable protective film via polymerization or decomposition reaction along the first charge is expected. In our previous work [30], it was shown that the glutaric anhydride additive is quite efficient to lower the self-discharge of $LiNi_{0.4}Mn_{1.6}O_4$ and the subsequent irreversible capacity loss. Indeed, no other family allowed reaching such passivation quality, as inferred from the resulting electrochemical performance. Therefore, glutaric anhydride appears as a good candidate to study the positive electrode passivation mechanisms.

Much of the processes and mechanisms taking place at the electrolyte/electrode interface still remain poorly understood, in particular for high potential materials. During the past few decades, substantial work has been done on analyzing the SEI and determining its composition [31–42], especially on negative electrodes such as graphite [31–35,38–40]. New lithium salt [43] and additives [27,28,44–47] for electrolyte and surface treatment [48] for active material were then evaluated in order to promote the formation of a stable passivation layer at the negative electrode, hence improving the electrochemical performance. More recently, interfacial problems at positive electrode leading to performance degradation of the battery upon aging and cycling were also identified [12,18,22,23,49–55]. The chemical, physical and structural properties of the interfacial layer at positive electrode, and its modification upon cycling, especially in the presence of an additive, still need further investigation.

In order to get further insight on the microstructure and local chemical composition of the interphase formed with or without the help of glutaric anhydride, $LiNi_{0.4}Mn_{1.6}O_4$ samples soaked in electrolyte were investigated by Transmission Electron Microscopy (TEM) and Electron Energy-loss Spectroscopy (EELS). In addition to the quantitative chemical analysis on a nanometric scale, analysis of the electron energy-loss near-edge structures can also provide additional information about the valence, coordination and site symmetry of the atom undergoing excitation [56]. Inhere, EELS spectra showing the O–K, Mn-$L_{2,3}$ and F–K edges were measured for the pristine and soaked samples. From these, Mn/O, F/Mn and Mn L_3/L_2 ratios were extracted and discussed.

Magic Angle Spinning NMR, as a local probe, provides information on the chemical and structural local environments of observed nuclei. Although its use is widespread in the field of materials for lithium batteries for structural characterization [57–62], only few studies deal with the investigation of surface layers and electrolyte decomposition products [23,53,54,63]. These studies proved the interest of using ^7Li NMR to detect and characterize the surface layer on a material, arising after contact with atmosphere or with the electrolyte of a lithium battery. In addition to be quantitative and non-destructive, one of the advantages of NMR is the possibility to separate clearly and unambiguously the signal arising from the passivation layer from the signal of the electrode active material [64,65]. Inhere, the growth and evolution of interphases are monitored by ^7Li and ^{19}F NMR. While quantitative ^7Li NMR was used to monitor both amount of lithiated interphase species and their interaction with the active material, ^{19}F NMR allowed discriminating fluorinated species such as LiF and fluorophosphates. Properties of the interphase are then discussed in the light of the influence of the electrochemical cycling and the use of glutaric anhydride as electrolyte additive. Obtained results are then put into perspective with respect to the rinsing of the sample before ex-situ analysis and the different adherence or dissolution properties displayed by LiF and fluorophosphates, respectively.

2. Experimental

$LiNi_{0.4}Mn_{1.6}O_4$ powders were obtained through the solid state reaction method described elsewhere [10]. Aged samples were obtained by soaking the pristine material for 5 min or 2 h in 1 M $LiPF_6$ in ethylene carbonate/dimethyl carbonate/propylene carbonate (EC/DMC/PC, 1/1/1) electrolyte, with and without 1% glutaric anhydride additive.

Previous work [5,30] performed in order to follow the evolution of the interphase upon cycling were done with an electrode formulation including PVdF, typically employed in most studies. However, the extremely intense sidebands of ^{19}F NMR PVdF signal at −211, −215 and −233 ppm mask almost any other fluorine signal from fluorinated species contained in the interphase. In these conditions, it is obviously difficult to follow the intensity changes of the LiF ^{19}F signal at −205 ppm and even impossible to detect and identify other fluorine containing species that may be present. Previous electrochemical measurements [66] have shown that the cycling performance of CMC-based and PVdF-based $LiNi_{0.4}Mn_{1.6}O_4$ electrodes are quite similar validating the use of fluorine-free binder, CMC-based electrodes to investigate the evolution of interphase fluorine species using ^{19}F NMR. Electrodes of $LiNi_{0.4}Mn_{1.6}O_4$ were then processed with Super P carbon (TIMCAL) as the conductive agent and CMC (DS = 0.7, Mw = 90,000 Aldrich) as binder, according to the electrode formulation: 85 wt. % active material, 10 wt. % Super P carbon and 5 wt. % CMC. After sonication of the slurry for 1 h, a drop of the slurry was deposited onto an aluminum current collector (area 1 cm^2) and dried at 100 °C in vacuum for 12 h to remove water solvent. The electrodes typically had an active material content of 8–10 mg cm^{-2}. Resulting electrodes were cycled in Swagelok™ cells, with a Li metal counter electrode at 0.2C regime using 1 M $LiPF_6$ (EC/DMC/PC, 1/1/1) electrolyte with or without 1% glutaric anhydride additive.

Rinsed electrodes were obtained by pouring two drops of DMC on them, just after opening the cells. Electrodes were then recovered before the undecomposed liquid electrolyte could dry on their surface. All electrodes were subsequently dried overnight under vacuum at 40 °C.

Following the work of Cuisinier et al. [63], TEM samples were prepared by a soft dry milling to avoid any further destruction of the interphase. Experiments were performed on a Hitachi HF 2000 (Field Emission Gun, 100 kV) with a probe diameter of 20 nm. In order to minimize carbon contamination and irradiation damage, samples were cooled down at liquid nitrogen temperature. Spectra

were recorded on a modified Gatan 666 parallel spectrometer equipped with a CCD camera and a Digipeels command. The energy resolution was 1.8 eV (given by the zero loss peak (ZLP) full width at half maximum) with a dispersion of 0.3 eV pixel^{-1}. Convergence and collection angles were respectively of 1.4 and 18.2 mrad. All spectra were dark count and gain corrected. Usually 8 areas per sample were measured to check for sample homogeneity. The acquisition time for each core-loss spectrum was 20 s. Prior to elemental quantification and manganese L_3/L_2 ratio analysis, spectra were first deconvoluted by the ZLP using PEELS software [67]. Low-loss spectrum was then used to remove the multiple-inelastic effects in the core-loss region using the Fourier ratio technique [68]. Background intensities at the O–K and Mn-L_{32} pre-edges regions were subtracted by fitting an inverse power-law function. The O/Mn ratios were corrected by the k-factor calculated from the pristine material [68]. For this purpose, a great care was taken to exclude fine structures of the O–K edge (pre-peak) in the choice of the windows for the O/Mn quantification. For the white-line L_3/L_2 ratio determination, we subtracted a calculated hydrogenic ionization cross-section σ_{L32} [68]. This was followed by area integration (from 638 eV to 648 eV and 648 eV–658 eV for the L_3 and L_2 edges respectively). In the present case, this method proved to provide less scattered results than more classical approaches including Gaussian or Lorentzian fits [69] due to the asymmetry of the L_3 edge shape for highly reduced Mn compounds [56].

^{7}Li and ^{19}F NMR measurements were carried out at room temperature on a Bruker Avance-500 spectrometer ($B0 = 11.8$ T, Larmor frequency $\nu_0 = 194.369$ MHz for ^{7}Li resonance and $\nu_0 = 470.592$ MHz for ^{19}F resonance). Single-pulse MAS spectra were obtained by using a Bruker MAS probe with a cylindrical 2.5 mm o.d. zirconia rotor. Spinning frequencies up to 25 kHz were used. A short single pulse length of 1 μs corresponding to a nonselective $\pi/2$ pulse was applied. For Li spectra, recycle time was in the 0.5 s range and a spectrometer dead time (preacquisition delay) of 5 μs was used before each acquisition. ^{19}F NMR spectra were acquired using a Hahn echo sequence to discard the significant contribution from the probe signal and a 5 s recycle time and a 3 μs pulse were used. The isotropic shifts, reported in ppm, are relative to an external reference made of 1 M aqueous solution of LiCl and CCl_3F set at 0 ppm for ^{7}Li and ^{19}F resonances, respectively. In order to perform a quantitative analysis, the different spectra were analyzed considering the total integrated intensity of the signal for each sample. The spectra displayed in this work were normalized taking into account the number of scans and the mass of sample. The notation of samples used in this work is described in Table 1.

3. Results and discussion

3.1. Contact with electrolyte

The particle size of pristine materials is in the order of micrometers, which is not suitable for TEM-EELS analysis. In order to also provide a larger surface area for the interphase to appear and its morphology and chemical composition to be determined, TEM/EELS experiments were carried out on samples ball-milled prior to soaking in electrolyte. In addition, since the binder-carbon clusters covering the surface disturbs the observation of the interphase, these experiments were performed on bare material and not on composite electrodes.

In Fig. 1, TEM micrographs are presented corresponding to both soaked samples (b) with and (a) without glutaric anhydride additive. As a result of ball milling, grains with various sizes and shapes are observed. A homogenous surface layer covering the whole surface of grains was in fact never evidenced in these TEM experiments. Deposits with a particular microstructure (amorphous-like, round-shape morphology) were observed (red circles in Fig. 1) instead, and seem to be trapped in between grains. EELS analyses were performed on these deposits to investigate their chemical composition.

EELS spectra for interfacial deposits on pristine, and soaked samples with and without additive, are presented in Fig. 2. Whereas the O–K (around 530 eV) and Mn-$L_{2,3}$ edges (around 640 eV) can be observed for the three samples, the F–K edge (around 690 eV) is only detected in the case of the soaked samples.

Table 1
Samples studied by MAS NMR. All electrodes were cycled between 3.5 and 5 V with a counter electrode of metallic lithium.

Sample	Electrolyte (additive)	Binder	Washing	Cycling experiment
Series 1	No	CMC	No	1 cycle
Series 2	Yes	CMC	No	1 cycle
Series 3	Yes	CMC	No	100 cycles
Series 4	Yes	CMC	Yes	100 cycles

Additive : glutaric anhydride; Washing agent : DMC.

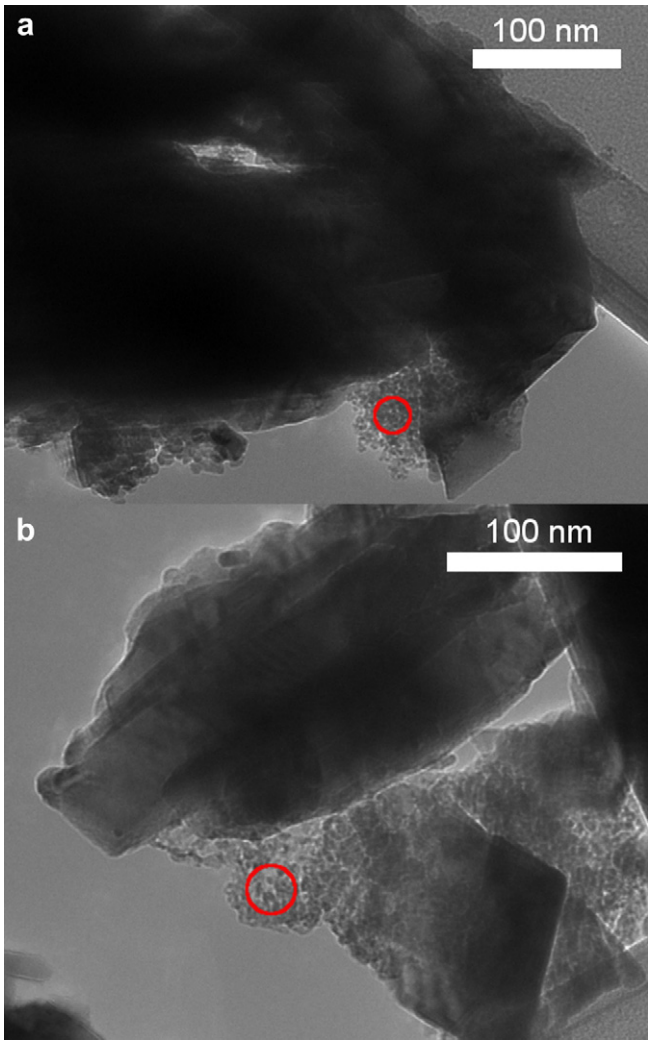

Fig. 1. TEM micrographs of the samples milled and soaked without (a) and (b) with additive. The probed areas are highlighted by red circles. (For interpretation of the references to colour in this figure legend, the reader is referred to the web version of this article.)

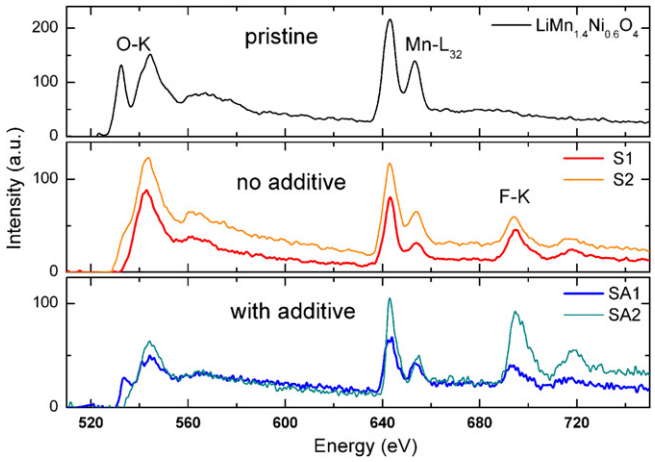

Fig. 2. EELS spectra ranging from 510 to 750 eV for the pristine and soaked materials (with and without additive). Two different areas are given in the case of soaked materials to reflect the disparity of the EELS spectra.

It thereby confirms the presence of the electrolyte and/or byproducts in these deposits. For each soaked sample, two spectra are shown to reflect the disparity of the EELS spectra, more particularly regarding the fine structures of the O–K edges. Indeed, for the pristine material the O–K edge exhibits a pre-peak at 532.4 eV which is attributed to the transition of the O 1s electron to the hybridized state of transition metal 3d and O 2p orbitals. [70,71] For the soaked samples, this pre-peak is observed either with a smaller intensity (spectra S2 and SA1 in Fig. 2) or is barely seen (S1 and SA2). When present, this pre-peak is also shifted towards higher energy (533.5 eV for SA1 for instance) thus showing the modification of the oxygen local environment compared to the pristine material and excluding the presence of pristine material in noticeable amount in the probed area. O–K edge is very sensitive to the ligand field which can give very important information about the chemical binding between the metal atom and ligand. According to literature [70,71], oxygen K edge pre-peak shifts to higher energy together with decreasing intensities indicate a lower oxidation state for the transition metal linked to these oxygen atoms.

From EELS spectra, O/Mn, F/O and Mn L_3/L_2 ratios were extracted and are reported in Table 2. The most striking result lies in the difference of L_3/L_2 ratios between the pristine and soaked samples. For the pristine material that exhibits almost an only Mn(IV) valence state, a ratio of 2.1 is found, in good agreement with the work of Wang et al. [72]. These results for the pristine material are extremely reproducible thus validating our method to extract Mn-L_{32} ratios. For both soaked samples, the L_3/L_2 ratios are similar and always higher than 2.1, thus corresponding to more reduced manganese compounds (Mn(III) or even lower [72]). This result highlights that the contact of the electrolyte with the starting material yields to the degradation of the active material, hence forming manganese-containing products that are trapped or included in the interphase. Since the Mn-L_3/L_2 ratios are similar for both soaked samples, it suggests that the additive has no or little influence on the manganese valence state of these manganese rich interphasial products.

Table 2
O/Mn, F/O and L_3/L_2 ratios deduced from EELS spectra. * The O/Mn ratios were corrected by the k-factor calculated from the pristine material.

Samples	O/Mn*	F/O	L_3/L_2
Pristine	2.5 ± 0.2	0	2.1 ± 0.1
Without additive	3.3 ± 0.2	0.7 ± 0.3	3.0 ± 0.6
With additive	2.4 ± 0.3	1.0 ± 0.5	3.1 ± 0.6

Although the proximity of the Mn-L_{32} edges with the F–K edge prevents a precise measurement of the fluorine K edge intensity, F/O ratios clearly appear extremely scattered, reflecting a sizeable inhomogeneity of the deposits. The O/Mn ratio for the soaked sample without additive is higher than for the soaked sample with additive. For the latter, values are close to those of the pristine material. The possible reasons for this apparent excess of oxygen will be discussed further on.

L_3/L_2 ratios as a function of F/O and O/Mn ratios are shown in Fig. 3a and b. There is a clear correlation between the F/O and Mn-L_{32} ratios: the more fluorine, the lower the manganese valence state is (high L_3/L_2 values). This observation suggests that the starting material is thus more degraded when large amounts of electrolyte decomposition products are present, allowing to correlate the two processes. Since the trend is similar for both soaked samples, the presence of additive does not seem to have a strong influence on this degradation. Nevertheless, transmission microscopy techniques probe on a very local scale and an absolute quantification of the total amount of manganese contained in the interphase is not possible. It is therefore not yet possible to conclude on the influence of additive on the dissolution/corrosion of the active material except that the phenomenon is not

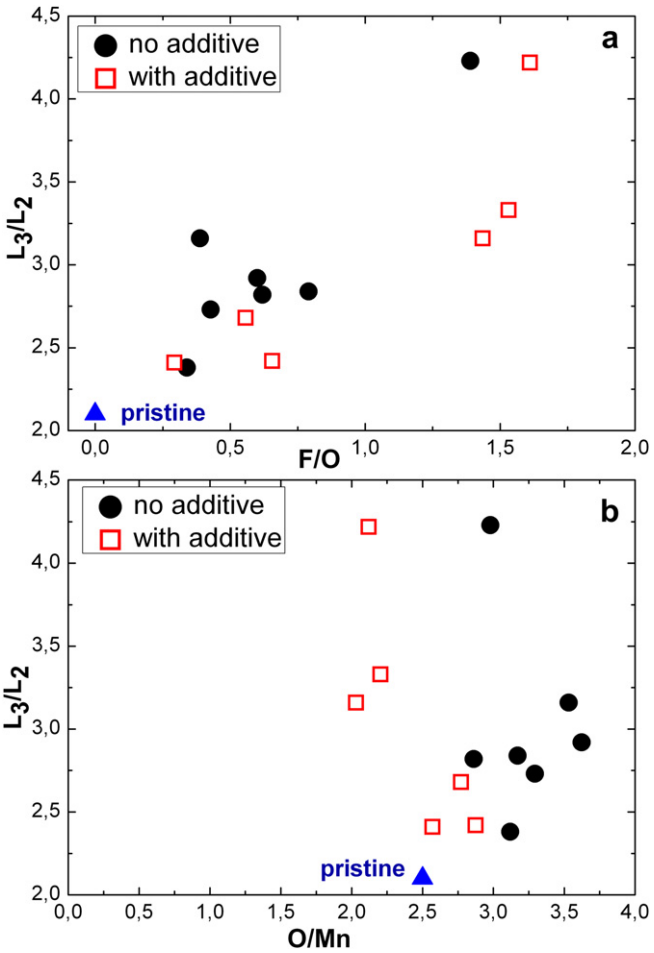

Fig. 3. Variation of L_3/L_2 ratio as a function of (a) F/O and (b) O/Mn ratios for the soaked samples with (red squares) and without additive (black circles). Data corresponding to the pristine material are added (blue triangles) as a reference. (For interpretation of the references to colour in this figure legend, the reader is referred to the web version of this article.)

completely suppressed. Due to the statistical dispersion, such influence could however be missed at this very local scale.

L_3/L_2 and O/Mn ratios do not seem to be correlated. The apparent excess of oxygen for the soaked sample without additive is therefore not correlated to the presence of manganese compounds in the interphase and should rather be attributed to oxygen containing organic species.

To obtain further information about the interphase composition, in particular on the evolution of the species coming from the decomposition of the $LiPF_6$ salt, ^{19}F and ^{7}Li NMR have been performed. ^{7}Li and ^{19}F NMR spectra of samples soaked for various amounts of time in the conventional $LiPF_6$ (1M EC:DMC 1:1) without additive are shown in Figs. 4a and 5a, respectively. The corresponding spectra of samples soaked in electrolyte with additive are shown in Figs. 4b and 5b, respectively. The evolution of the ^{7}Li integrated intensity for the corresponding spectra is displayed in Fig. 6a. The increase of the ^{7}Li intensity reflects the ongoing deposition of lithiated species with soaking time. This trend is observed for both electrolytes with and without additive although it appears to be exacerbated when the additive is not present in the electrolyte. The higher amount of lithiated species detected for the additive-free electrolyte is consistent with our previous work [30]. The integrated ^{19}F NMR intensities of surface LiF and $Li_xPF_y/Li_xPO_yF_z$ signals were quantified by fitting the spectra using the software

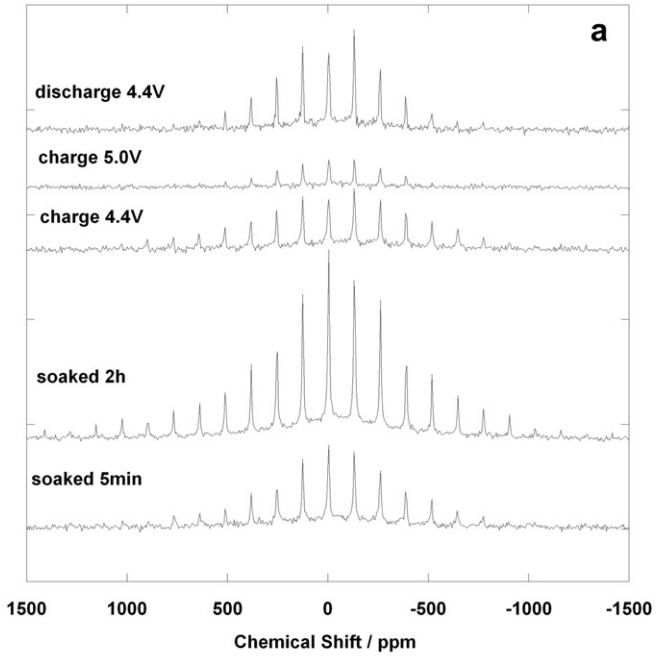

Fig. 4. Normalized ^{7}Li MAS NMR spectra for (a) Series 1 (no additive) and (b) Series 2 (with additive).

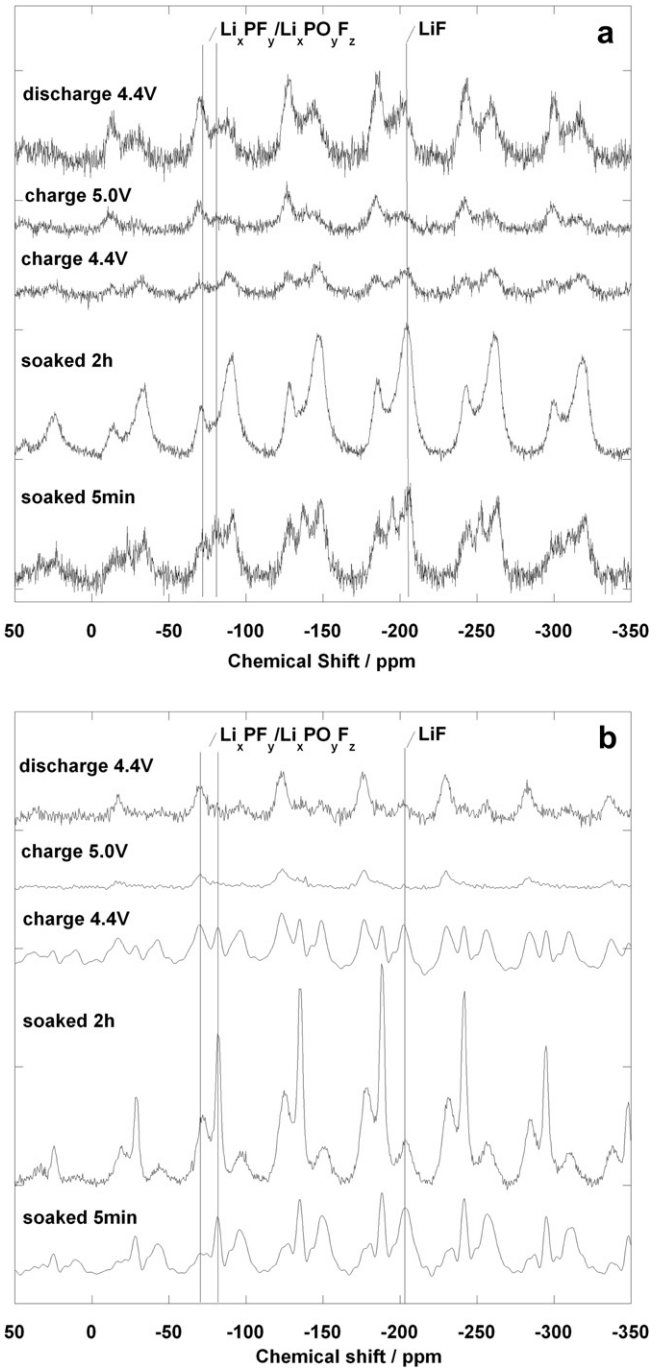

Fig. 5. Normalized ^{19}F MAS NMR spectra for (a) Series 1 (no additive) and (b) Series 2 (with additive).

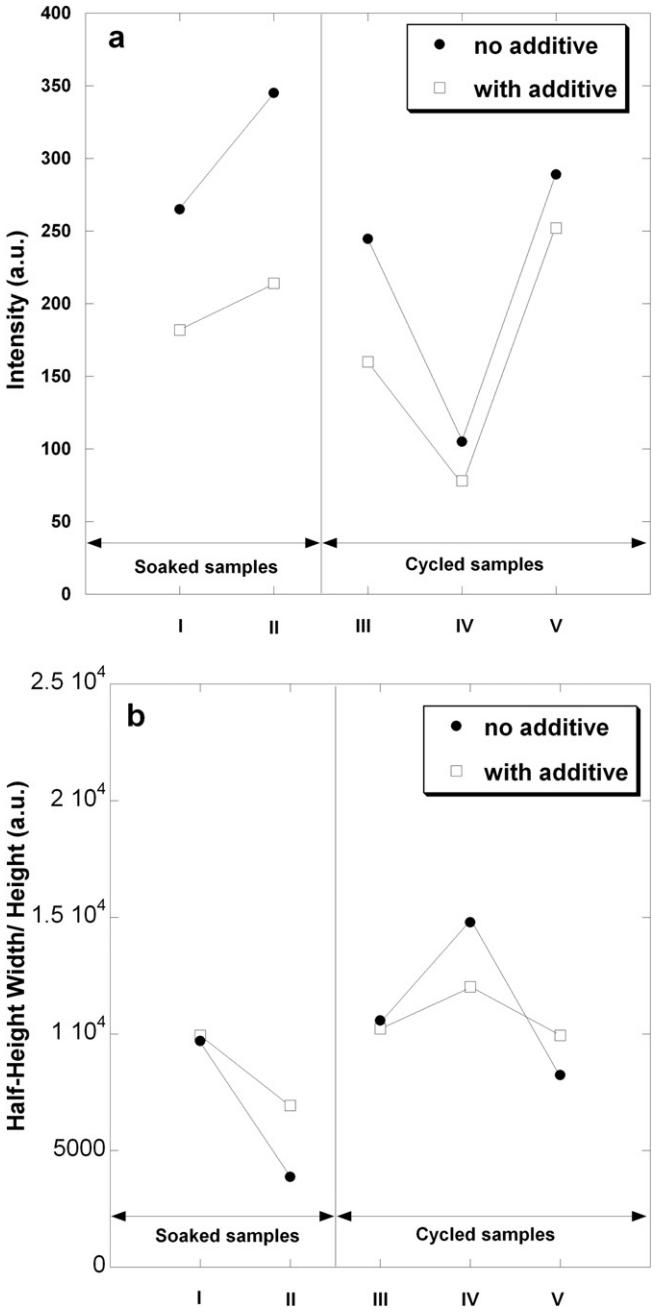

Fig. 6. Evolution of the (a) normalized integrated intensities of ^{7}Li MAS NMR spectra depending on different electrochemical situations for Series 1 and 2. (b) FWHM of ^{7}Li NMR spectra normalized to the height depending on different electrochemical situations for Series 1 and 2. *I: soaked 5min; II: soaked 2 h; III: the first charge to 4.4 V; IV: first charge to 5.0 V; V: subsequent discharge to 4.4 V.

DMfit2010 [73] and values are reported in Table 3. For the sample soaked in the additive-free electrolyte for 5 min, 52% of the ^{19}F NMR signal rises at −205 ppm (Table 3 and Fig. 5a) and corresponds to LiF. Two other broad resonances are detected at −72 and −80 ppm and assigned to $Li_xPF_y/Li_xPO_yF_z$ fluorophosphates [74]. The signal assigned to LiF clearly increases with soaking time, reaching 63% after 2 h and, suggesting that the increase of the intensity observed in ^{7}Li NMR corresponds mainly to LiF formation.

Similar species are detected for samples soaked in electrolyte with or without additive, namely LiF and fluorophosphates (Fig. 5). Corresponding TEM/EELS experiments indicate that fluorine K-edge

Table 3
Percentages fluorine in LiF and $LiP_yF_z/Li_xPO_yF_z$ for the CMC electrodes series 3 and series 4.

	No additive		With additive	
Sample	LiF %	$LiP_yF_z/Li_xPO_yF_z$ %	LiF %	$LiP_yF_z/Li_xPO_yF_z$ %
Soaked 5 min	52	48	48	52
Soaked 2 h	63	37	30	70
Charge 4.4 V	52	48	10	90
Charge 5.0 V	50	50	4	96
Discharge 4.4 V	40	60	26	74

fine structures are, unfortunately, not characteristic enough to allow a definitive attribution on the chemical environment of fluorine in the interphase. Nevertheless, obvious differences between the additive electrodes and additive-free electrodes appear on the ^{19}F NMR spectra (Fig. 5a and b) allowing discrimination between these two types of species. As a matter of fact, a larger amount of fluorophosphates is observed for both soaked samples when glutaric anhydride is added to the electrolyte. Indeed, the signals ascribed to fluorophosphates dominate the LiF signal and represents 52 and 70% after 5 min and 2 h, respectively. These results indicate clearly the preferential formation of fluorophosphates when glutaric anhydride is used, even for a plain exposure with the electrolyte. While the reaction of $LiPF_6$ with trace water leads typically to deposits of mostly LiF, a non-negligible amount of fluorophosphates would require the organic solvent molecules or the additive molecules to be involved in the reaction. Therefore, the observed change in the composition of the interphase then suggests that glutaric anhydride either promotes a reaction involving the solvents of the electrolyte or reacts with the salt or its decomposition products to form these fluorophosphates.

The excess of oxygen detected in the interphase by EELS for the additive-free electrolyte may be due to either a higher ratio of organic species in the interphase, to a higher amount of interphase on the surface or to the presence of different organic molecules containing a higher number of oxygen atoms. The first possibility can be ruled out since a higher amount lithiated species, and in particular LiF, is measured in the case of the additive-free electrolyte. Fluorophosphates are typically coming from the decomposition of the electrolyte, involving inorganic salt as well as the solvent [75]. Therefore, a higher amount of organic byproducts can also be expected when more fluorophosphates are formed. This is not the case for the additive-free electrolyte. This is in agreement with XPS results published elsewhere [30] indicating the formation of a thicker organic interphase after an extended exposure or cycling, when the additive is used. Thus, the second hypothesis can be also ruled out and it seems reasonable to ascribe the oxygen excess to the different nature of the organic species coming from the decomposition depending on the addition of glutaric anhydride. It appears therefore that the use of glutaric anhydride leads not only to a preferential formation of fluorophosphates but also alters the nature of the organic species contained in the interphase.

3.2. Electrochemical cycling

Considering now the evolution of the interphase upon the first electrochemical cycle, the ^{7}Li NMR signal after the first charge to 5 V is lower than those observed at 4.4 V during the first charge and the subsequent discharge (Fig. 4). It suggests that interphase species are partially destroyed or contain less lithium species after an exposure at high potential. This process seems, in addition, to be reversible. This result is also in agreement with the data obtained from the PVdF electrodes [30] indicating a lower ^{7}Li integrated intensity after 14 days of rest in the charged state with respect to a single charge, confirming the existence of a high potential

phenomenon corresponding to either a partial destruction of the interphase or a decrease of the interphase lithium content. Comparing the width of sidebands manifold between soaked and cycled samples (Fig. 6b), it is worth noting two different types of profiles. Cycled samples show a broader sidebands manifold profile while soaked samples show a thinner and sharper profile. Considering the higher integrated intensity observed for the soaked samples, it seems reasonable, in that case, to ascribe the change of profile of the sidebands manifold to the amount of lithiated species stacked on the surface of the active material [64,76] but no change in the interaction between the interphase and the active material surface can be evidenced here. Further comparison of the profiles of sidebands manifold will be discussed in the following.

The quantification of integrated ^{19}F NMR intensities of surface species (Table 3) does not lead to significant variation of LiF and $Li_xPO_yF_z$ percentages for electrodes charged to 4.4 V in an additive-free electrolyte with respect to the electrode soaked for 5 min in the electrolyte. Indeed, after the first charge to 4.4 V, the ^{19}F signal of LiF (52%) still dominates that of $Li_xPF_y/Li_xPO_yF_z$ (48%). The integrated intensity is much lower with respect to the soaked samples, in agreement with ^{7}Li results. On the contrary, there is a clear change in the interphase composition for the electrode after an oxidation to 5 V. The major signal seems to correspond to $Li_xPF_y/Li_xPO_yF_z$ fluorophosphates.

The total amount of detected fluorine does not change significantly from charge 4.4 V–5 V. Combined with the decrease of intensity observed in ^{7}Li NMR, this result seems to be consistent with the transformation or conversion of LiF to $Li_xPF_y/Li_xPO_yF_z$ and a decreasing Li/F ratio. Moreover, the formation of fluorophosphates is irreversible as the subsequent discharge down to 4.4 V does not change this situation back and ^{19}F signals are still arising mainly from fluorophosphates. The discharge to 4.4 V seems then to lead to an increase of the amount of fluorophosphates on the surface of the active material particles characterized by an increase of both ^{7}Li and ^{19}F integrated intensities.

The evolutions of the integrated intensities of ^{7}Li NMR spectra of cycled samples (Fig. 6a) follow the same trend, whether the additive is used or not, and although there is always less intensity when additive is used. Again, a larger amount of fluorophosphates in the interphase composition is noticed on the ^{19}F NMR spectra for electrodes cycled in the presence of additive (Fig. 5 and Table 3). Moreover, the signals ascribed to fluorophosphates clearly dominate (90%) the LiF signal (10%) after the first charge to 4.4 V. This result confirms that glutaric anhydride is actually promoting the formation of fluorophosphates.

After a charge to 5.0 V, the ^{19}F signal corresponding to LiF almost disappears but is detected again after the subsequent discharge to 4.4 V, although the intensity is quite low. Considering the signal to noise ratio, it is not possible to completely rule the presence of LiF at 5.0 V out. This seems to indicate that the LiF formed by simple contact between electrodes and electrolyte is decomposed or dissolved at high potential, possibly to be partially converted in fluorophosphates. It seems that LiF is then formed again during the reduction process. A change in the respective intensities of signals at −70 and −80 ppm can also be noticed between soaked and cycled samples. As a matter of fact, the intensity at −80 ppm is much higher than that at −70 ppm for the soaked samples as opposed to the cycled ones. Thus, although fluorophosphates seem to be promoted by the presence of glutaric anhydride in the electrolyte, there is still a clear influence of the potential applied to the sample on the type of fluorophosphates formed.

The evolution of the widths of the ^{7}Li sidebands manifold (Fig. 6b) has a much lower magnitude in the case of electrodes cycled in the presence of glutaric anhydride. This indicates that the overall change in the interaction between Li in the interphase and the surface of the active material is occurring with a lesser extent compared to the case of the additive-free electrolyte. Since the amount of surface lithium is changing upon aging or cycling, this evolution suggests that lithium species formed or removed along the dissolution/deposition processes, are more homogenously distributed on the surface of the active material and exhibit a more pronounced trend to cover its surface instead of stacking on the top of each other.

On the contrary, for the electrodes cycled without additive, larger fluctuations of widths are observed, exhibiting a minimum for the sample soaked for 2 h and a maximum for sample oxidized to 5 V. These two points correspond to the maximum and minimum of lithium amount, respectively. For all samples soaked or cycled without additive, the FWHM decreases when the amount of lithium increases, consistent with the stacking of lithiated species and significant variations of thickness characteristic of a more inhomogenous interphase layer.

Put together, these results are in agreement with the data obtained for PVdF electrodes [30] indicating that glutaric anhydride restrains the formation of lithiated species due to the decomposition of electrolyte and leads to a more homogenous interphase. In addition, glutaric anhydride alters the chemical composition of the interphase by promoting the formation of $Li_xPF_y/Li_xPO_yF_z$ rather than LiF, known to be resistive.

In order to investigate the stability of the interphase upon an extended cycling, ^{7}Li (Fig. 7a) and ^{19}F (Fig. 7c) NMR were performed on electrodes cycled with additive for different cycle numbers. Normalized intensities are compared before and after the rinsing process using DMC (Fig. 7b and d). After rinsing the electrodes with DMC, the observed ^{7}Li NMR (Fig. 7b) intensities are quite different for the electrodes after 1 cycle and 100 cycles while the intensities stay extremely low and of comparable magnitudes for the sample after 1 charge.

The corresponding ^{19}F spectra (Fig. 7c) indicate that the main component after 1 cycle and 100 cycles, prior to rinsing, corresponds to LiF. Other broad components of the spectra that can be found between −70 and −80 ppm are assigned to $Li_xPF_y/Li_xPO_yF_z$ although a weak contribution from pristine $LiPF_6$ cannot be rule out. After rinsing, most of the LiF (Fig. 7d) is gone but the fluorophosphates are still observed, suggesting a higher stability on the surface of the active material. This is confirmed by spectra corresponding to 1 charge. The ^{19}F spectrum of the electrode before any rinsing process displays mostly fluorophosphates and LiF is barely detected. The ^{19}F and ^{7}Li spectra (Fig. 7b and d) acquired after rinsing with DMC show no significant change in the interphase composition. ^{19}F signals are mainly assigned to fluorophosphates and no significant change in integrated intensity can be noticed. These results show unambiguously the effect of rinsing and indicate that LiF coming from the decomposition of the electrolyte is mostly removed by this process.

In addition, comparing the sample after 1 cycle and those after of 30 and 100 cycles, the overall integrated intensity of surface lithiated species is found to be lower after a longer cycling although the signal increases between 30 and 100 cycles. These results support the LiF formation and partial removal during cycling, so that it accumulates as it is confirmed by the increase of the ^{19}F signal corresponding to LiF between 30 and 100 cycles. In comparison, no significant evolution can be observed between rinsed electrodes after 1 and 100 cycles, confirming the good stability of the formed fluorophosphates towards cycling.

First, these rinsing experiments allow evidencing that interphase layers can have different adherence to the active material, depending on their compositions. LiF is mostly removed by the preparation of samples for ex-situ analysis. These experiments therefore shed light on the great care that has to be taken when analyzing samples using ex-situ techniques, as it can alter conclusions. In the light of the comparison of electrodes from series 1 and

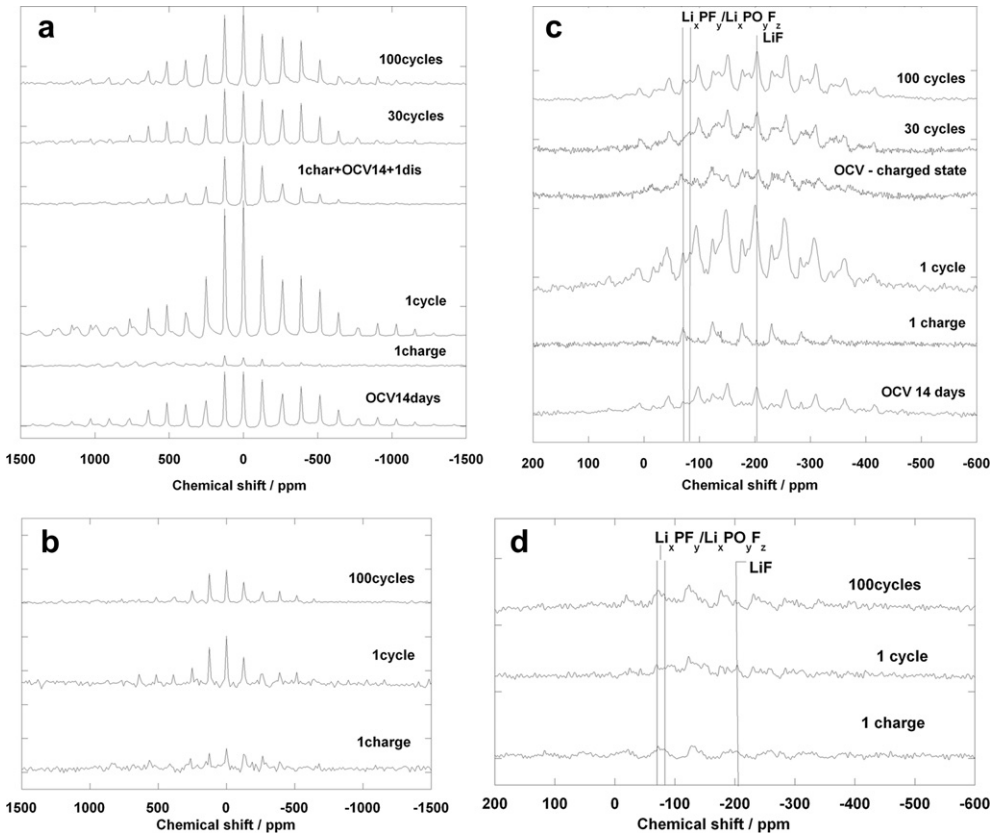

Fig. 7. Normalized ^{7}Li MAS NMR spectra for (a) Series 3 (not washed) and (b) Series 4 (washed). Normalized ^{19}F MAS NMR spectra for (c) Series 3 (not washed) and (d) Series 4 (washed).

series 2, conclusions about the influence of the glutaric anhydride on the composition of the interphase have to be put in perspective. Although the formation of fluorophosphates seems to be promoted, it appears that LiF is still formed in significant amount but most of it is actually washed out and removed by the DMC rinsing during the preparation of samples for ex-situ analysis. LiF is known to be quite resistive and the better electrochemical performance could have been mistakenly assigned only to a lower amount of inorganic fluorinated species when glutaric anhydride is used. In fact, the addition of glutaric anhydride to the electrolyte seems to lead to an interphase composition which is more resistant to dissolution in DMC, whether inside the battery along the cycling process or during the rinsing process prior to analysis. This work confirms also that modifying the interphase architecture and/or composition is possible and efficient to improve the electrochemical performance of existing systems.

4. Conclusions

Combined TEM/EELS and MAS NMR allowed giving further insights on the chemistry of the interphase formed on the surface of $LiNi_{0.4}Mn_{1.6}O_4$ from its reaction with liquid $LiPF_6$ electrolyte as well as on the modifications brought by the use of glutaric anhydride additive.

The reactions occurring at the electrode/electrolyte are clearly modified by the presence of glutaric anhydride as the formation of fluorophosphates is promoted. NMR proved to be very efficient in probing the interphase. Nevertheless, degradation of the active material, leading to the presence of manganese within the interphase and invisible to NMR, could be evidenced by complementary TEM/EELS. As a matter of fact, the clear correlation between the increasing amount of fluorinated species on the surface and the lower valence of Mn suggests that a chemical reaction, rather than a physical adsorption, produces the interphase. It appears that the use of glutaric anhydride change the composition of the interphase but does not stop the degradation of the active material. According to the results of ^{7}Li and ^{19}F NMR, glutaric anhydride additive promotes a more homogenous interphase containing more Li_xPF_z/$Li_xPO_yF_z$ fluorophosphates. In addition, these species seem to be more stable on the surface of active material, as shown by rinsing experiments. This better stability of Li_xPF_z/$Li_xPO_yF_z$ compared to LiF on $LiNi_{0.4}Mn_{1.6}O_4$ surface might yield a better protection and a more efficient passivation layer. In particular, the destruction of the LiF component of the interphase at high potential might lead to the exposure of bare surface of $LiNi_{0.4}Mn_{1.6}O_4$ to the electrolyte and to subsequent interfacial reactions and an important self-discharge. Altering the composition of the interphase by promoting more stable fluorophosphates seems to be a good way to circumvent this high potential phenomenon. These results lead to an improved understanding of the stability of interphase and the influence of an additive, on the characteristics of the interphase.

Acknowledgments

The authors are grateful to Dr. Anne-Claire Gaillot for TEM imaging of some samples and fruitful discussions.

References

[1] J.B. Goodenough, Y. Kim, Chem. Mater. 22 (2010) 587.
[2] E. Ferg, R.J. Gummow, A. de Kock, M.M. Thackeray, J. Electrochem. Soc. 141 (1994) L147.
[3] T. Ohzuku, A. Ueda, N. Yamamoto, J. Electrochem. Soc. 142 (1995) 1431.
[4] A. Jansen, A.J. Kahaian, K.D. Kepler, P.A. Nelson, K. Amine, D.W. Dees, D.R. Vissers, M.M. Thackeray, J. Power Sources 81-82 (1999) 902.

[5] R. Dedryvère, D. Foix, S. Franger, S. Patoux, L. Daniel, D. Gonbeau, J. Phys. Chem. C 114 (2010) 10999.
[6] C. Sigala, D. Guyomard, A. Verbaere, Y. Piffard, M. Tournoux, Solid State Ionics 81 (1995) 167.
[7] C. Sigala, A. Verbaere, J.L. Mansot, D. Guyomard, Y. Piffard, M. Tournoux, J. Solid State Chem. 132 (1997) 372.
[8] K. Amine, H. Tukamoto, H. Yasuda, Y. Fujita, J. Power Sources 68 (1997) 604.
[9] Q. Zhong, A. Bonakdarpour, M. Zhang, Y. Gao, J.R. Dahn, J. Electrochem. Soc. 144 (1997) 205.
[10] S. Patoux, L. Daniel, C. Bourbon, H. Lignier, C. Pagano, F.L. Cras, S. Jouanneau, S. Martinet, J. Power Sources 189 (2009) 344.
[11] S. Patoux, L. Sannier, H. Lignier, Y. Reynier, C. Bourbon, S. Jouanneau, F. Le Cras, S. Martinet, Electrochim. Acta 53 (2008) 4137.
[12] K. Edström, T. Gustafsson, J.O. Thomas, Electrochim. Acta 50 (2004) 397.
[13] T. Eriksson, A.M. Andersson, C. Gejke, T. Gustafsson, J.O. Thomas, Langmuir 18 (2002) 3609.
[14] D. Aurbach, B. Markovsky, Y. Talyossef, G. Salitra, H.J. Kim, S. Choi, J. Power Sources 162 (2006) 780.
[15] D. Aurbach, B. Markovsky, G. Salitra, E. Markevich, Y. Talyossef, M. Koltypin, L. Nazar, B. Ellis, D. Kovacheva, J. Power Sources 165 (2007) 491.
[16] H. Duncan, D. Duguay, Y. Abu-Lebdeh, I.J. Davidson, J. Electrochem. Soc. 158 (5) (2011) A537.
[17] E. Peled, J. Electrochem. Soc. 126 (1979) 2047.
[18] Kang Xu, Energies 3 (2010) 135.
[19] D. Aurbach, K. Gamolsky, B. Markovsky, G. Salitra, Y. Gofer, U. Heider, R. Oesten, M. Schmidt, J. Electrochem. Soc. 147 (2000) 1322.
[20] S.S. Zhang, K. Xu, T.R. Jow, J. Electrochem. Soc. 149 (2002) A1521.
[21] S.S. Zhang, K. Xu, T.R. Jow, J. Electrochem. Solid-State Lett. 5 (2002) A92.
[22] N. Dupré, J.-F. Martin, J. Oliveri, D. Guyomard, A. Yamada, R. Kanno, Electrochem. Comm. 10 (12) (2008) 1897.
[23] N. Dupré, J.-F. Martin, J. Oliveri, P. Soudan, A. Yamada, R. Kanno, D. Guyomard, J. Power Sources 196 (2011) 4791.
[24] S. Song, S. Baek, Electrochem. Solid-State Lett. 12 (2009) A2.
[25] S. Song, R. Reade, E. Cairns, J. Vaughey, M. Thackeray, K. Striebel, J. Electrochem. Soc. 151 (2004) A1012.
[26] K. Xu, C.A. Angell, J. Electrochem. Soc. 145 (1998) L70.
[27] A. Abouimrane, I. Belharouak, K. Amine, Electrochem. Comm. 11 (2009) 1073.
[28] K. Xu, S. Ding, T.R. Jow, J. Electrochem. Soc. 146 (1999) 4172.
[29] S.A. Zhang, J. Power Sources 162 (2006) 1379.
[30] Z. Wang, N. Dupré, R. Dedryvere, S. Franger J.- F. Martin, L. Daniel, S. Patoux, D. Guyomard, submitted for publication J. Electrochem Soc.
[31] D. Aurbach, B. Markovsky, A. Shechter, Y. Ein-Eli, H. Cohen, J. Electrochem. Soc. 143 (1996) 3809.
[32] D. Aurbach, M.D. Levi, E. Levi, A. Schechter, J. Phys. Chem. B 101 (1997) 2195.
[33] Y. Ein-Eli, B. Markovsky, D. Aurbach, Y. Carmeli, H. yamin, S. Luski, Electrochim. Acta 39 (1994) 2559.
[34] Z.-X. Wang, X.-J. Huang, L.-Q. Chen, J. Electrochem. Soc. 151 (10) (2004) A1641.
[35] R. Dedryvere, S. Laruelle, S. Grugeon, L. Gireaud, J.-M. Tarascon, D. Gonbeau, J. Electrochem. Soc. 152 (4) (2005) A689.
[36] R. Dedryvere, L. Gireaud, S. Grugeon, J.-M. Tarascon, D. Gonbeau, J. Phys. Chem. B 109 (2005) 15868.
[37] D. Bar-Tow, E. Peled, L. Burstein, J. Electrochem. Soc. 146 (1999) 824.
[38] E. Peled, D. Golodnitsky, C. Menachem, D. Bar-Tow, J. Electrochem. Soc. 145 (1998) 3482.
[39] E. Peled, D. Bar Tow, A. Merson, A. Gladkich, L. Burstein, D. Golodnitsky, J. Power Sources 97–98 (2001) 52.
[40] K.-I. Morigaki, A. Ohta, J. Power Sources 76 (1998) 159.
[41] G.R.V. Zhuang, P.N. Ross, Electrochem. Solid State Lett. 6 (2003) A136.
[42] P. Verma, P. Maire1, P. Novák, Electrochim. Acta 55 (2010) 6332.
[43] K. Xu, S.S. Zhang, U. Lee, J.L. Allen, T.R. Jow, J. Power Sources 146 (2005) 79.
[44] C. Taubert, M. Fleischhammer, M. Wolfhart-Mehrens, U. Wietelmann, T. Buhrmester, J. Electrochem. Soc. 157 (2010) 13.
[45] W. Li, B.L. Lucht, J. Power Sources 168 (2007) 258.
[46] S. Santee, A. Xiao, L. Yang, J. Gnanaraj, B.L. Lucht, J. Power Sources 194 (2009) 1053.
[47] W. Li, A. Xiao, B.L. Lucht, M.C. Smart, B.V. Ratnakumar, J. Electrochem. Soc. 155 (9) (2008) A648.
[48] H. Buqa, P. Golob, M. Winter, J.O. Besenhard, J. Power Source 97-98 (2001) 122–125.
[49] D. Aurbach, M.D. Levi, E. Levi, H. Teller, B. Markovsky, G. Salitra, L. Heider, J. Electrochem. Soc. 145 (9) (1998) 3024.
[50] B.P. Abraham, R.D. Twesten, M. Balasubramanian, I. Petrov, J. McBreen, K. Amine, Electrochem. Comm. 4 (2002) 620.
[51] D. Mori, H. Kobayashi, M. Shikano, H. Nitani, H. Kageyama, S. Koike, H. Sakaebe, K. Tatsumi, J. Power Sources 189 (2009) 676.
[52] M. Koltypin, D. Aurbach, L. Nazar, B. Ellis, J. Power Sources 174 (2007) 1241.
[53] N. Dupré, J.-F. Martin, J. Oliveri, P. Soudan, D. Guyomard, A. Yamada, R. Kanno, J. Electrochem. Soc. 156 (5) (2009) C180–C185.
[54] N. Dupré, J.-F. Martin, D. Guyomard, A. Yamada, R. Kanno, J. Power Sources 189 (2009) 557.
[55] L. El Ouatani, R. Dedryvère, C. Siret, P. Piensan, D. Gonbeau, J. Electrochem. Soc. 156 (6) (2009) A468.
[56] L.A.J. Garvie, A.J. Craven, Phys. Chem. Min. 21 (1994) 191.
[57] C.P. Grey, N. Dupré, Chem. Rev. 104 (2004) 4493.
[58] J. Bréger, N. Dupré, P.J. Chupas, P.L. Lee, T. Proffen, J.B. Parise, C.P. Grey, J. Am. Chem. Soc. 127 (2005) 7529.
[59] B. Key, R. Bhattacharyya, M. Morcrette, V. Seznéc, J.-M. Tarascon, C.P. Grey, J. Am. Chem. Soc. 131 (2009) 9239.
[60] E. Bekaert, F. Robert, P.E. Lippens, M. Ménétrier, J. Phys. Chem. C 114 (2010) 6749.
[61] D. Carlier, M. Blangero, M. Ménétrier, M.l Pollet, J.-P. Doumerc, C. Delmas, Inorg. Chem. 48 (2009) 7018.
[62] M. Ménétrier, I. Saadoune, S. Levasseur, C. Delmas, J. Mat. Chem. 9 (1999) 1135.
[63] M. Cuisinier, J.F. Martin, P. Moreau, T. Epicier, R. Kanno, D. Guyomard, N. Dupré, Solid State Nucl. Magn. Reson. 42 (2012) 51.
[64] M. Ménétrier, C. Vaysse, L. Croguennec, C. Delmas, C. Jordy, F. Bonhomme, P. Biensan, Electrochem. Solid State Lett. 7 (2004) A140.
[65] N. Dupré, J.F. Martin, A. Yamada, R. Kanno, D. Guyomard, J. Mat. Chem. 18 (2008) 4266.
[66] Z. Wang, N. Dupré, B. Lestriez, J.-F. Martin, L. Daniel, S. Patoux, D. Guyomard, Electrochim. Acta 62 (2012) 77.
[67] P. Fallon, C.A. Walsh, Computer Code PEELS, University of Cambridge, England, 1996.
[68] R.F. Egerton, Electron Energy Loss Spectroscopy in the Electron Microscope, second ed. Plenum, New York, 1996.
[69] T. Riedl, T. Gemming, K. Wetzig, Ultramicroscopy 106 (2006) 191.
[70] H. Kurata, C. Colliex, Phys. Rev. B 48 (4) (1993) 2102.
[71] W.S. Yoon, Clare P. Grey, M. Balasubramanian, X.Q. Yang, D.A. Fischer, J. McBreen, Electrochem. Solid State Lett. 7 (3) (2004) A53.
[72] Z.L. Wang, J.S. Yin, Y.D. Jiang, Micron 31 (2000) 571.
[73] D. Massiot. http://nmr.cemhti.cnrs-orleans.fr/dmfit/.
[74] A.V. Plakhotnyk, L. Ernst, R. Schmutzler, J. Fluorine Chem. 126 (2005) 27.
[75] l. Yang, B. Ravdel, B.L. Lucht, Electrochem. Solid State Lett. 13 (8) (2010) A95.
[76] N. Dupré, J. Oliveri, J.F. Martin, A. Yamada, R. Kanno, D. Guyomard, J. Electrochem. Soc. 156 (5) (2009) C180.